

Unsteady Heat and Mass Transfer Slip Flow over an Exponentially Permeable Stretching Sheet

M. A. Islam^{1,2*}, M. Y. Ali², S. M. O. Gani^{1,2}

¹Department of Natural Science, Port City International University, Chattogram 4217, Bangladesh

²Department of Mathematics, Chittagong University of Engineering and Technology, Chattogram 4217, Bangladesh

Received 8 September 2021, accepted in final revised form 8 February 2022

Abstract

In this paper, the problem of unsteady two-dimensional boundary layer heat and mass transfer flow over an exponentially stretching sheet embedded in a porous medium in the presence of a uniform magnetic field with thermal radiation, heat generation/absorption, and suction/blowing is analyzed numerically. Instead of no-slip boundary conditions, velocity slip, thermal slip, and mass slips at the boundary are considered. Using a suitable similarity transformation, the governing partial differential equations are transformed to a system coupled with nonlinear ordinary differential equations. The reduced equations are solved numerically by using `bvp4c` with the MATLAB package. A detailed parametric study is performed to illustrate the physical parameters on the velocity, temperature, and concentration profile and the local skin-friction coefficient and Nusselt and Sherwood number. Then the results are exhibited in both graphical and tabular forms. It is observed that the present results have been in close agreement with the previously published studies under some special cases.

Keywords: Unsteady flow; Exponentially stretching sheet; Thermal radiation; Heat generation/absorption.

© 2022 JSR Publications. ISSN: 2070-0237 (Print); 2070-0245 (Online). All rights reserved.
doi: <http://dx.doi.org/10.3329/jsr.v14i2.55577> J. Sci. Res. **14** (2), 443-457 (2022)

1. Introduction

The boundary layer flow with heat and mass transfer over a stretching sheet of a viscous fluid has received considerable interest because of its various applications in hot rolling, polymer extrusion from a dye, metal extrusion, metal spinning, spinning of filaments, wire drawing, glass fiber production, crystal growing, paper production, continuous casting, cooling of a large metallic plate in a bath, which can be an electrolyte, etc. Altogether in these cases, a study of the flow and heat transfer can be of great importance since the ultimate product depends largely on the surface heat transfer rate and the skin-friction coefficient [1]. Sakiadas [2] first studied the two-dimensional boundary layer flow on a moving continuous solid surface. Crane [3] first investigated the boundary layer flow due

* Corresponding author: aminulislampciu88@gmail.com

to a linearly stretching sheet. Many investigators like Gupta and Gupta [4], Grubka and Bobba [5], Elbashbeshy [6], Andersson [7] analyzed heat transfer and flow on a continuous moving stretching surface under different conditions such as suction or blowing, variable temperature, variable surface heat flux, slip condition. Boundary layer flow and heat transfer over an exponentially stretching surface have wider applications in technology like drawing, annealing, and thinning of copper wires. Magyari and Keller [8], Elbashbeshy [9], Partha *et al.* [10], Sanjayanand and Khan [11] considered the exponentially stretching sheet in their study. The study of utilizing heat generation or absorption in moving fluids assumes an excellent significance altogether situations that deal with exothermic and endothermic reactions and those concerned with dissociating fluids. The effects of fluid heat generation or absorption are important in applying certain porous media. The attention of researchers has been focused on thermal radiation as a mode of energy transfer due to its vital applications in processes involving high temperatures like hypersonic flights, rocket combustion chambers, missile re-entry, power plants for interplanetary flight, and gas-cooled nuclear reactors [12]. The magneto hydrodynamic boundary layer flow of an electrically conducting fluid has wide applications in engineering problems like nuclear reactors, heat energy extraction, plasma studies, MHD generator, and oil exploration. Again, unsteady flows, like start-up processes and periodic fluid motion, are very much important in engineering practices. The unstable environment occurs in several engineering problems like the cascades of blades of turbo-machinery, the ship propeller, and helicopter rotor [13]. Hence, it is important to analyze the simultaneous effects of unsteadiness, magnetic field, heat source or sink, and thermal radiation. Sekar *et al.* [14] studied the heat source effect on unsteady mixed convection flow through a very narrow parallel plate channel in a porous medium with an external transverse magnetic field. Hussain and Ahmad [15] discussed the unsteady MHD boundary layer flow of Newtonian fluids over an exponentially stretching sheet with heat source effects.

The process of suction and blowing even have their importance in many engineering activities, for instance, within the design of thrust bearing and radial diffusers and thermal oil recovery. Suction is applied to chemical processes to get rid of reactants. Blowing is employed to feature reactants, which cool the surface, prevent corrosion or scaling and reduce the drag [16]. The assumption that a liquid adheres to a solid boundary is known as a no-slip boundary condition. Partial velocity slip (the non-adherence of the fluid to a solid boundary) may take place on the stretching boundary when the fluid is unpurified, like emulsions, suspensions, foams, and polymer solutions. The polishing of artificial heart valves and internal cavities are some examples of fluids presenting boundary slip. For a few coated surfaces, like Teflon, resist adhesion, the no-slip condition is replaced by Navier's partial slip condition, where the slip velocity is proportional to the local shear stress [17]. Recently, Bhattacharyya *et al.* [18] investigated the slip effect on boundary layer mixed convection flow from a vertical plate. Sreenivasulu *et al.* [19] analyzed the slip effects on MHD flow and heat transfer over an exponential permeable stretching surface with suction, joule heating, thermal radiation, and viscous dissipation. Zaman *et*

al. [20] studied the effects of velocity and thermal slip on MHD boundary layer flow over an exponentially stretching sheet with suction, radiation, heat source, and chemical reaction. Chaudhary and Choudhary [21] described the double slip effects on MHD flow and heat transfer over an exponentially stretching surface with thermal radiation, viscous dissipation, joule heating, and suction or blowing.

In view of the above discussions and motivated by the paper of Mukhopadhyay [17], an attempt is made to study the multiple slip effects along with the effects of heat generation or absorption and thermal radiation on unsteady hydromagnetic fluid over an exponentially stretching sheet embedded in a porous medium with suction or blowing. We introduce similarity transformations to convert the governing partial differential equations to a set of nonlinear ordinary differential equations, which are then solved numerically using the `bvp4c` function in MATLAB software. The effect of the involved parameters is demonstrated through graphs and Tables.

2. Mathematical Formulation of the Problem

An unsteady two-dimensional hydromagnetic boundary layer flow of an incompressible viscous electrically and radiating fluid over an exponentially permeable stretching sheet is considered. We measure the x -axis along the stretching surface in the direction of motion, and the y -axis is perpendicular to it. The flow is generated by the stretching sheet such that the velocity of the boundary sheet is of exponential order of the flow directional coordinate x . A uniform magnetic field $\mathbf{B}(t) = \mathbf{B}_0(1 - t)^{-1/2}e^{x/2}$ of strength \mathbf{B}_0 is applied normally to the sheet, which generates the magnetic effect in the x axis and where we take the reference length $L = 1$ and a positive constant with dimension reciprocal time $\alpha = 1$. The magnetic Reynolds number is small, so we can neglect the induced magnetic field. The governing continuity, momentum, energy, and concentration equations are written as:

$$\frac{\partial u}{\partial x} + \frac{\partial v}{\partial y} = 0 \tag{1}$$

$$\frac{\partial u}{\partial t} + u \frac{\partial u}{\partial x} + v \frac{\partial u}{\partial y} = \nu \frac{\partial^2 u}{\partial y^2} - \frac{\sigma B^2}{\rho} u - \frac{\nu}{K_1} u \tag{2}$$

$$\frac{\partial T}{\partial t} + u \frac{\partial T}{\partial x} + v \frac{\partial T}{\partial y} = \frac{\kappa}{\rho C_p} \frac{\partial^2 T}{\partial y^2} - \frac{1}{\rho C_p} \frac{\partial q_r}{\partial y} + \frac{1}{\rho C_p} Q_0(T - T_\infty) \tag{3}$$

$$\frac{\partial C}{\partial t} + u \frac{\partial C}{\partial x} + v \frac{\partial C}{\partial y} = D_m \frac{\partial^2 C}{\partial y^2} \tag{4}$$

Here u and v are the velocity components along the x axis and y axis respectively, t is the time, $\nu (= \mu/\rho)$ is the kinematic fluid viscosity, μ is the co-efficient of fluid viscosity, ρ is the density, σ is the electric conductivity of the fluid, K_1 is the permeability of the porous medium, T is the temperature of the fluid, κ is the thermal conductivity, C_p is the

specific heat at constant pressure, q_r is the radiative heat flux, Q_0 is the heat generation co-efficient, C is the concentration of the fluid and D_m is the co-efficient of mass diffusivity. In order to correlate the radiation field with the flow field, a source term (W/m³), named radiative power per unit volume, is added to the energy balance equation of the flow. The radiative power per unit volume is defined as the negative derivative of radiation heat flux q_r . Using Rosseland approximation [22], the Radiation heat flux q_r is written as

$$q_r = -\frac{4\sigma^* \partial T^4}{3K^* \partial y} \quad (5)$$

where σ^* and K^* are the Stefan-Boltzman constant and the absorption coefficient, respectively. The difference in the temperature within the flow is considered to be sufficiently small such that T^4 can be expanded in Taylor's series about a free stream temperature T_∞ and neglecting the higher-order terms beyond the first degree in $(T - T_\infty)$, we get $T^4 \cong 4T_\infty^3 T - 3T_\infty^4$

Then the equation (3) becomes:

$$\frac{\partial T}{\partial t} + u \frac{\partial T}{\partial x} + v \frac{\partial T}{\partial y} = \frac{\kappa}{\rho C_p} \frac{\partial^2 T}{\partial y^2} + \frac{16\sigma^* T_\infty^3}{3\rho C_p K^*} \frac{\partial^2 T}{\partial y^2} + \frac{1}{\rho C_p} Q_0 (T - T_\infty) \quad (6)$$

The associate boundary conditions are

$$\begin{aligned} u &= U(x, t) + Nv \frac{\partial u}{\partial y}, \quad V = -V(x, t), \quad T = T_w(x, t) + E \frac{\partial T}{\partial y}, \\ C &= C_w(x, t) + F \frac{\partial C}{\partial y}, \quad \text{at } y = 0 \\ u &\rightarrow 0, \quad T \rightarrow T_\infty, \quad C \rightarrow C_\infty \quad \text{as } y \rightarrow \infty \end{aligned} \quad (7)$$

where $U(x, t) = \frac{U_0}{1-t} e^x$ is the stretching sheet velocity, $T_w(x, t) = T_\infty + \frac{T_0}{(1-t)^2} e^{x/2}$ is the stretching surface temperature, $C_w(x, t) = C_\infty + \frac{C_0}{(1-t)^2} e^{x/2}$ is the concentration of the stretching surface, T_∞ is the temperature far away from the stretching surface with $T_w > T_\infty$, C_∞ is the concentration far away from the stretching surface with $C_w > C_\infty$, U_0 is the reference velocity, T_0 is the reference temperature, C_0 is the reference concentration, N is the velocity slip factor, E is the thermal slip factor, F is the mass slip factor and $V(x, t) = V_0(1-t)^{-1/2} e^{x/2}$ is the suction or injection velocity, V_0 is the strength of suction or blowing. The velocity, thermal, and mass slip factor are considered as follows:

$$N = N_1(1-t)^{1/2} e^{-x/2}, \quad E = E_1(1-t)^{1/2} e^{-x/2}, \quad F = F_1(1-t)^{1/2} e^{-x/2}$$

where N_1, E_1 and F_1 are the initial values of velocity, thermal, and mass slip factors, respectively. The condition of the no-slip case is obtained when $N = E = F = 0$.

For the solution of momentum and energy equations (2) and (3), we introduce the following dimensionless variables:

$$\eta = \sqrt{\frac{U_0}{2\nu(1-t)}} e^{x/2} y, \quad \psi = \sqrt{\frac{2U_0\nu}{1-t}} e^{x/2} f(\eta)$$

$$T = T_\infty + \frac{T_0}{(1-t)^2} e^{x/2} \theta(\eta), \quad C = C_\infty + \frac{C_0}{(1-t)^2} e^{x/2} \phi(\eta)$$

Introducing dimensionless similarity variables into the governing equations (2)-(4), we get the following system of ordinary differential equations:

$$f''' + f f'' - 2 f'^2 - A e^{-X} (2f' + \eta f'') - (M + K)f' = 0 \tag{8}$$

$$\left(1 + \frac{4}{3} R\right) \theta'' + \text{Pr}(f \theta' - f' \theta) - A \text{Pr} e^{-X} (4\theta + \eta \theta') + Q_H \text{Pr} e^{-X} \theta = 0 \tag{9}$$

$$\phi'' + \text{Sc}(f \phi' - f' \phi) - A \text{Sc} e^{-X} (4\phi + \eta \phi') = 0 \tag{10}$$

The Boundary conditions in equation (5) are reduced to the corresponding boundary condition for velocity, temperature, and concentration fields are as:

$$f(0) = S, f'(0) = 1 + \lambda f''(0), \theta(0) = 1 + \delta \theta'(0),$$

$$\phi(0) = 1 + \gamma \phi'(0) \text{ at } \eta = 0$$

$$f'(\infty) \rightarrow 0, \theta(\infty) \rightarrow 0, \phi(\infty) \rightarrow 0 \text{ as } \eta \rightarrow \infty \tag{11}$$

where the prime denotes the differentiation w.r.t η . Also

$$A = \frac{1}{U_0}, X = x, M = \frac{2\sigma B_0^2}{\rho U_0}, K = \frac{2\nu}{K_0 U_0}, R = \frac{4\sigma^* T_\infty^3}{\kappa K^*}, \text{Pr} = \frac{\rho C_p \nu}{\kappa},$$

$$Q_H = \frac{Q_0(1-t)}{U_0 \rho C_p}, \text{Sc} = \frac{\nu}{D_m}, S = \frac{V_0}{\sqrt{\frac{U_0 \nu}{2}}}, \lambda = N_1 \sqrt{\frac{U_0 \nu}{2}}, \delta = E_1 \sqrt{\frac{U_0}{2\nu}} \text{ and } \gamma = F_1 \sqrt{\frac{U_0}{2\nu}}$$

are the unsteadiness parameter, dimensionless coordinate, magnetic parameter, permeability of the porous medium, radiation parameter, Prandtl number, heat generation ($Q_H > 0$) and absorption ($Q_H < 0$) parameter, Schmidt number, suction parameter, velocity, thermal, and mass slip parameter, respectively.

The Skin-friction co-efficient, Nusselt number, and Sherwood number, which are the physical quantities of interest in this problem, are defined by

$$C_f = \frac{2\tau_w}{\rho U^2}, \quad N_{u_x} = \frac{x q_w}{k(T_w - T_\infty)} \quad \text{and} \quad S_{h_x} = \frac{x J_w}{D(C_w - C_\infty)} \tag{12}$$

Where τ_w is the surface shear stress, q_w is surface the heat flux and J_w is the mass flux, and those are given by

$$\tau_w = \mu \left(\frac{\partial u}{\partial y}\right)_{y=0}, \quad q_w = -k \left(\frac{\partial T}{\partial y}\right)_{y=0} \quad \text{and} \quad J_w = -D \left(\frac{\partial C}{\partial y}\right)_{y=0} \tag{13}$$

$$C_f = \sqrt{2x} (Re_x)^{-\frac{1}{2}} f''(0), \quad N_{u_x} = -\sqrt{\frac{x}{2}} \sqrt{Re_x} \theta'(0) \quad \text{and} \quad S_{h_x} = -\sqrt{\frac{x}{2}} \sqrt{Re_x} \phi'(0) \tag{14}$$

where $Re_x = \frac{xU}{\nu}$ is the local Reynolds number.

3. Result and Discussion

The nonlinear ordinary differential equations (8) to (10) and the boundary conditions are solved numerically using bvp4c with MATLAB package. The obtained results represent the influences of the several non-dimensional governing parameters, namely magnetic parameter (M), unsteadiness parameter (A), porosity parameter (K), suction/blowing parameter (S), velocity slip parameter (λ), radiation parameter (R), heat generation/absorption parameter (Q_H), Prandtl number (Pr), thermal slip parameter (δ), Schmidt number (Sc), and mass slip parameter (γ) on the velocity, temperature, and concentration profiles. The computed numerical values of Nusselt number $[-\theta'(0)]$ are presented in Table 1 and are compared with the published results of Magyari and Keller [8], Elbashbeshy *et al.* [9], and Mukhopadhyay [17]. The results are found in close agreement. The influences of the Skin-friction co-efficient, Nusselt number, and Sherwood number are shown in Tables 2, 3, and 4. For numerical computations, $X = 1.5, A = 0.1, M = 0.3, K = 0.5, R = 0.2, Pr = 5, Sc = 1, S = 0.2, Q_H = \delta = \gamma = 0.3, \lambda = 0.05$ and $\eta = 2$ are considered. These values are treated as common throughout this study, except the numerous values in respective figures and Tables.

Table 1. Comparison values of $[-\theta'(0)]$ for, $A = M = K = R = Sc = S = \lambda = Q_H = \delta = \gamma = 0$.

Pr	Magyari and Keller [8]	Elbashbeshy et al. [9]	Mukhopadhyay [17]	Present Results
3	1.8691	1.86907	1.8691	1.9355
5	2.5001	2.50013	2.5001	2.4684
10	3.6604	3.66037	3.6603	3.5739

3.1. Velocity profiles

The effects of various parameters on the velocity are represented in Figs.1-5. Figure 1 illustrates the influence of magnetic parameter M on the velocity profile. It is seen that velocity decreases as the magnetic parameter increases. A resisting force named Lorentz force generated due to magnetic field reduces the motion of the fluid within the boundary layer region. It is observed from Fig. 2 that velocity increases with the increment in the unsteadiness parameter A . Fig. 3 shows the effect of the suction/blowing parameter at the stretching sheet on the fluid velocity. It is noted that velocity decreases with increasing suction parameter ($S > 0$), whereas velocity is seen to extend with blowing ($S < 0$).

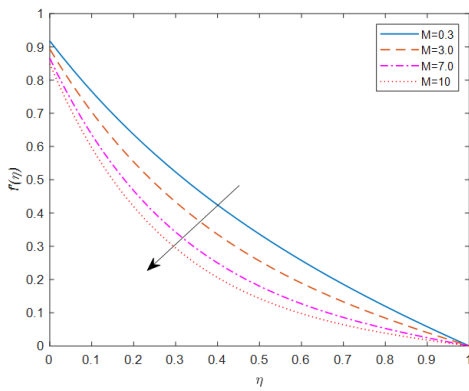


Fig. 1. Velocity profile for different values of Magnetic parameter M .

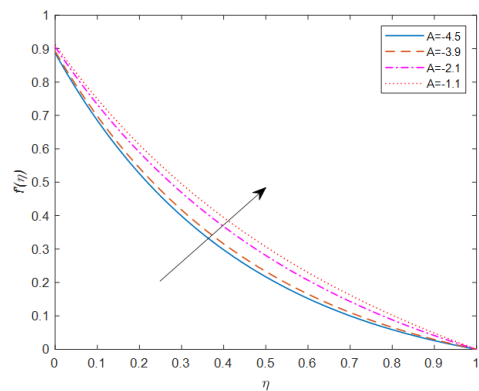


Fig. 2. Velocity profile for different values of the unsteadiness parameter A .

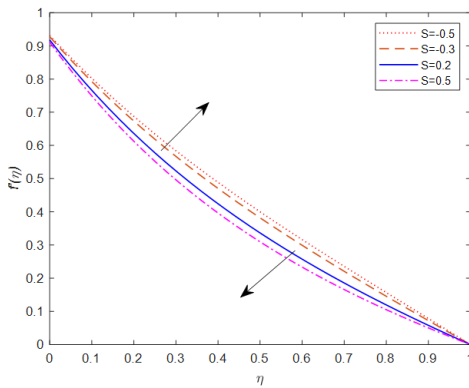


Fig. 3. Velocity profile for different values of Suction parameter S .

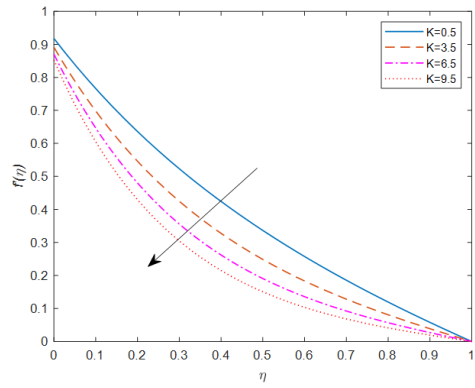


Fig. 4. Velocity profile for different values of the Porosity parameter K .

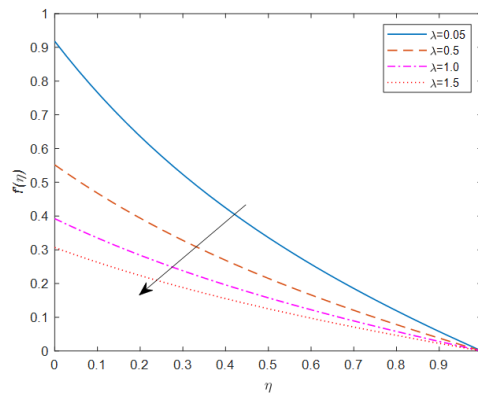


Fig. 5. Velocity profile for different values of velocity slip parameter.

Fig. 4 depicts the effect of the porosity parameter K on the velocity profile. Fluid velocity decreases with the rise in the values of the porosity parameter. Increases in porosity parameter dilated the porous layer of the flow, which increased the velocity boundary layer thickness. The velocity profile for various values of the velocity slip parameter λ is displayed in figure 5. It is found that velocity reduces because the velocity slip parameter enhances.

3.2. Temperature profiles

Figs. 6-14 display the behaviors of temperature profiles for the consequences of varied parameters. The effect of magnetic parameters on temperature profiles is plotted in Fig. 6, which shows that temperature increases with a rise within the magnetic parameter (M). Fig. 7 exhibits the effect of the unsteadiness parameter on the temperature profile. We observe that temperature increases because the unsteadiness parameter (A) increases. It is found from Fig. 8 that fluid temperature decreases with the increasing values of the suction parameter ($S > 0$), but it increases owing to blowing ($S < 0$). Fig. 9 describes the effect of the porosity parameter K on the temperature profile. It is certain that fluid temperature increases with increases in the porosity parameter. Fig. 10 reveals the influence of the radiation parameter on the temperature profile. It is noticed that temperature increases because the radiation parameter (R) increases. So, we should always control radiation at its minimum to facilitate a better cooling environment. Fig. 11 depicts the influence of the Prandtl number on the temperature profile. It is seen that fluid temperature decreases with the Prandtl number (Pr) increase. The nature of the temperature profile for various values of heat generation and absorption parameter is presented in Fig. 12. It is noteworthy that the increase in heat generation ($Q_H > 0$) parameter enhances the fluid temperature, whereas the opposite trend is found in the case of heat absorption ($Q_H < 0$).

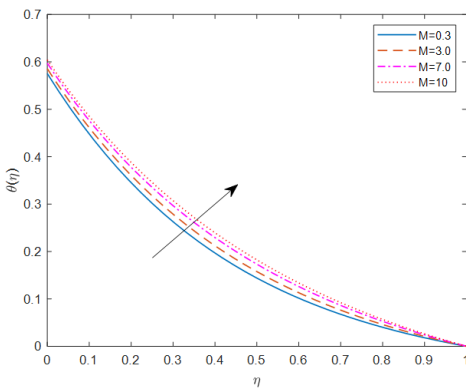


Fig. 6. Temperature profile for different values of Magnetic parameter M .

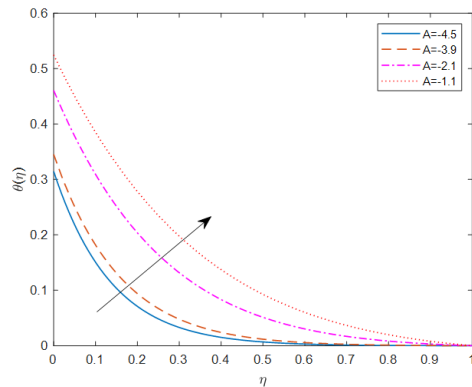


Fig. 7. Temperature profile for different values of Unsteadiness parameter A .

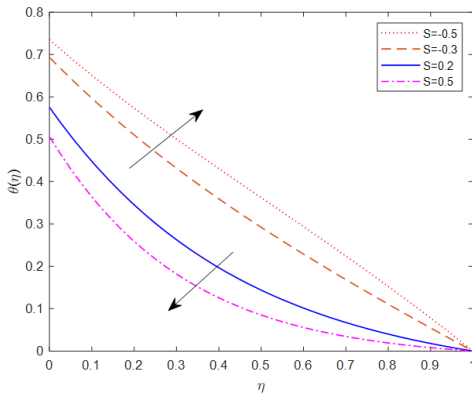


Fig. 8. Temperature profile for different values of Suction parameter S .

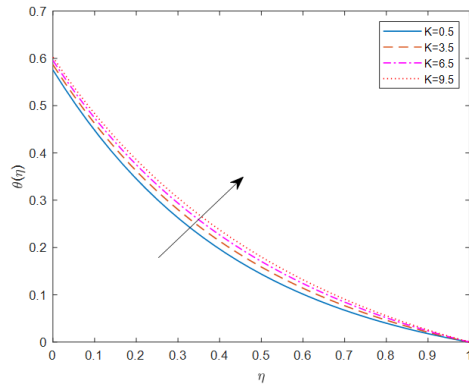


Fig. 9. Temperature profile for different values of Porosity parameter K .

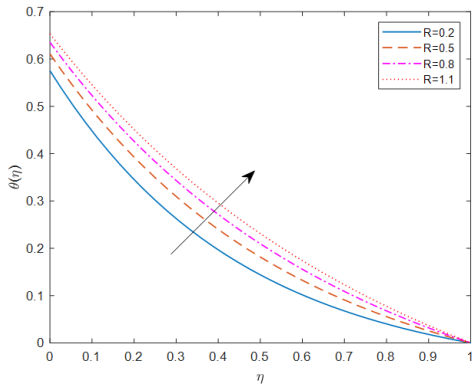


Fig. 10. Temperature profile for different values of radiation parameter R .

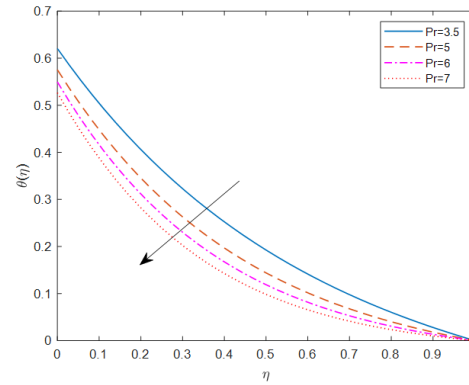


Fig. 11. Temperature profile for different values of Prandtl number Pr .

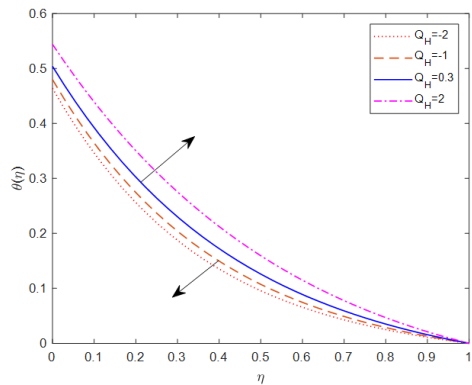


Fig. 12. Temperature profile for different values of heat generation parameter Q_H .

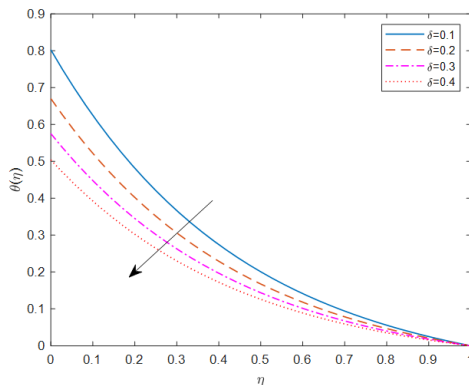


Fig. 13. Temperature profile for different values of thermal slip parameter δ

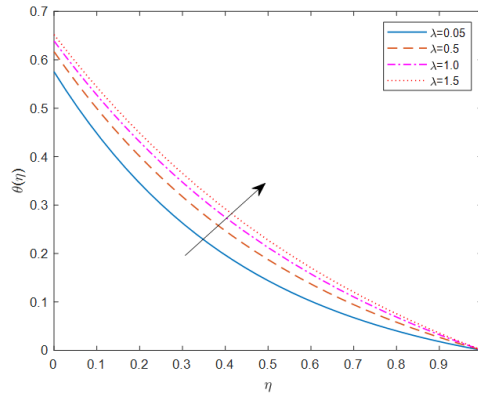


Fig. 14. Temperature profile for different values of velocity slip parameter λ .

Fig. 13 shows the temperature profile variation against the thermal slip parameter. It is observed that the temperature profile decreases with the thermal slip parameter (δ). With the increase of thermal slip parameter, less heat is transferred to the fluid from the sheet, and then the temperature decreases. It is revealed from Fig. 14 that fluid temperature increases on increasing velocity slip parameter.

3.3. Concentration profiles

The nature of the concentration profile for the effects of the varied parameter is discussed in Figs. 15-21. The dimensionless concentration profiles for several magnetic and unsteadiness parameter values are presented in Figs. 15 and 16, respectively. These two figures conclude that concentration decreases with the increase in both the magnetic (M) and unsteadiness parameter (A), respectively. Fig. 17 demonstrates the variation of concentration profile against suction and blowing parameters. It is observed that concentration reduces with the enhancement of the suction parameter ($S > 0$), but the opposite trend is seen just in the case of blowing ($S < 0$).

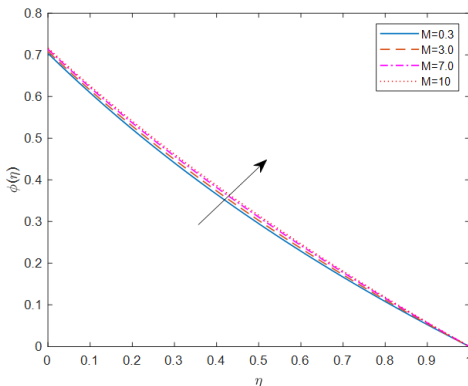


Fig. 15. Concentration profile for different values of Magnetic parameter M .

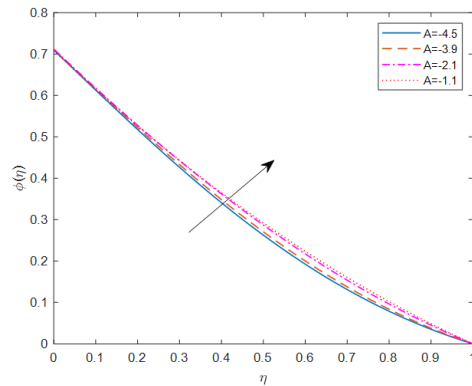


Fig. 16. Concentration profile for different values of the unsteadiness parameter A .

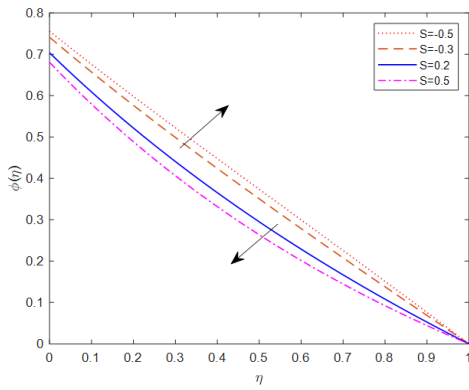


Fig. 17. Concentration profile for different values of suction parameter S .

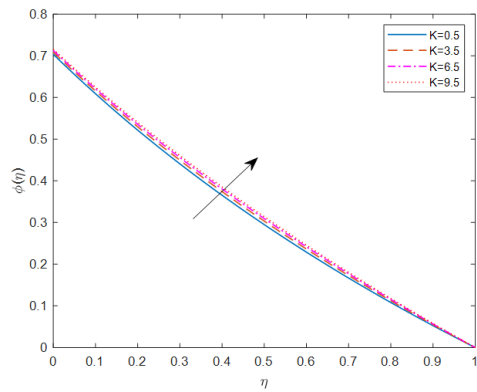


Fig. 18. Concentration profile for different values of Porosity parameter K .

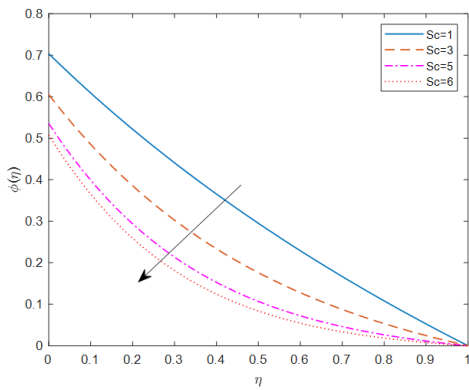


Fig. 19. Concentration profile for different values of Schmidt number Sc .

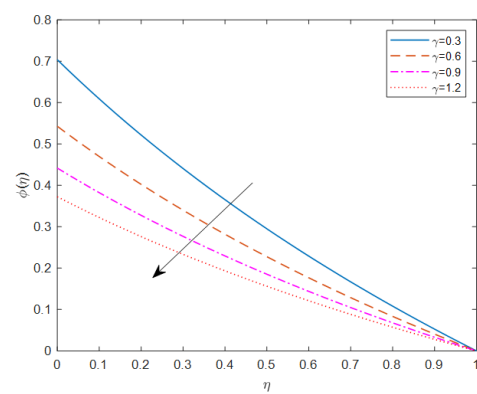


Fig. 20. Concentration profile for different values of mass slip parameter γ .

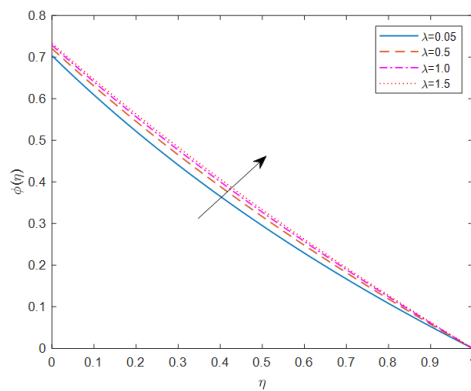


Fig. 21. Concentration profile for different values of velocity slip parameter λ .

Fig. 18 illustrates the effects of the porosity parameter on the concentration profile of the flow. It is evident from the figure that an increase in the porosity parameter (K) enhances the concentration profile. Fig. 19 depicts the influence of Schmidt number on concentration profile. It is found that concentration decreases as the Schmidt number (Sc) increases. Fig. 20 exhibits the effect of mass slip parameter on concentration profile. We notice that concentration reduces with the increase of mass slip parameter (γ). Fig. 21 shows the effect of the velocity slip parameter on concentration profile. It is seen that the velocity slip parameter (λ) boosts up concentration profile.

3.4. Skin friction coefficient, Nusselt and Sherwood number

The effects of suction, velocity slip, thermal slip, and mass slip parameter on velocity, temperature, and concentration gradient are displayed in Figs. 22-24. Fig. 22 describes the variation of the velocity gradient $f''(0)$ against suction for different values of velocity slip parameter. The skin friction coefficient increases are due to increase λ . Fig. 23 illustrates the effect of the thermal slip parameter on the local temperature gradient against the suction parameter. An increase in the thermal slip parameter decreases the local Nusselt number. Fig. 24 shows the nature of the mass transfer rate against suction for increasing values of mass slip parameter. It is seen that the local Sherwood number is decreased.

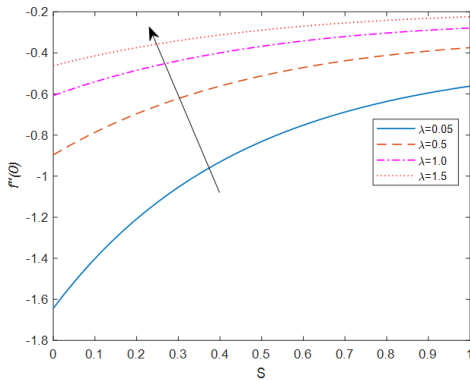


Fig. 22. Velocity gradient against suction parameter for different values of velocity slip parameter λ .

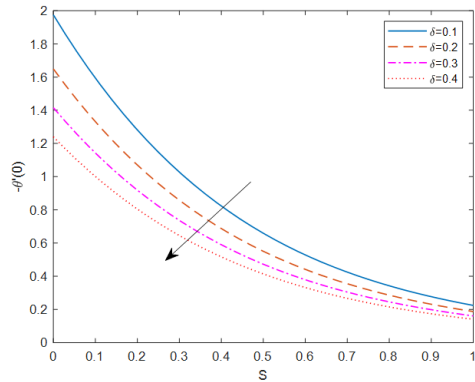


Fig. 23. Temperature gradient against suction parameter S for different values of thermal slip parameter δ .

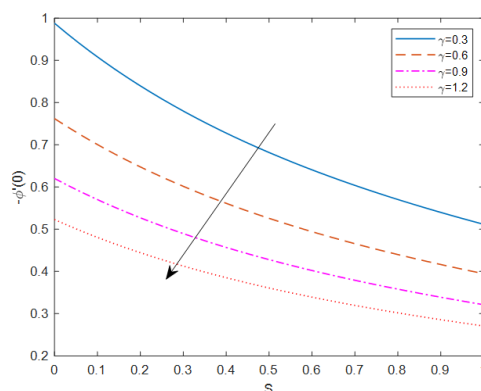


Fig. 24. Concentration gradient against suction parameter for different values of mass slip parameter γ .

Table 2. Sherwood Number for different values of Sc and γ .

Parameter	Values	$-\phi'(0)$
Sc	3	1.3159
	5	1.5482
	6	1.6405
γ	0.6	0.7620
	0.9	0.6202
	1.2	0.5229

Table 3. Nusselt number for different values of R, Pr, Q_H and δ .

Parameter	Values	$-\theta'(0)$
R	0.2	1.4157
	0.5	1.2976
	0.8	1.2158
Pr	3.5	1.2652
	6	1.5018
	7	1.5786
Q_H	-2	1.3398
	-1	1.3003
	2	1.1398
δ	0.1	1.9749
	0.2	1.6492
	0.4	1.2401

The numerical values of skin friction coefficient, Nusselt, and Sherwood Number are presented in Tables 2-4. We observe from Table 4 that the Skin friction coefficient increases with the increasing values of A, λ whereas decreases with the increasing values of M, K and S . It is seen from Tables 3 and 4 that Nusselt number increases with the increasing values of S and Pr whereas decreases with the increasing values of M, A, K, λ, R, Q_H and δ . It is revealed from Tables 2 and 4 that the Sherwood number increases with the increasing values of S and Sc whereas decreases with the increasing values of M, A, K, λ and γ .

Table 4. Skin friction coefficient, Nusselt, and Sherwood Number for different M, A, K, S, and λ .

Parameter	Values	$f''(0)$	$-\theta'(0)$	$-\phi'(0)$
M	0.3	-1.6434	1.4157	0.9879
	3	-2.1283	1.3815	0.9718
	7	-2.6792	1.3427	0.9549
A	-4.5	-2.2679	2.2849	0.9677
	-3.9	-2.1644	2.1827	0.9599
	-2.1	-1.8942	1.7978	0.9605
K	3.5	-2.1755	1.3782	0.9703
	6.5	-2.5932	1.3487	0.9574
	9.5	-2.9381	1.3248	0.9475
S	-0.5	-1.3722	0.8826	0.8145
	-0.3	-1.4453	1.0221	0.8627
	0.5	-1.7725	1.6454	1.0650
λ	0.5	-0.8966	1.2772	0.9316
	1	-0.6076	1.2036	0.9049
	1.5	-0.4621	1.1597	0.8900

4. Conclusion

A numerical study is presented to discuss the effects of slip-on unsteady MHD boundary layer flow, heat, and mass transfer over an exponentially stretching sheet in a porous medium in the presence of thermal radiations, heat generation/absorption, and suction/blowing.

The main outcomes of the current study are as follows:

- The velocity profile is reduced with the rise in velocity slip parameter, whereas the temperature and concentration profile enhance for large values of velocity slip parameter.
- The magnetic and porosity parameter decline the velocity profiles and enhance the temperature and concentration profiles.
- Skin friction coefficient increases for velocity slip and unsteadiness parameters, whereas it reduces for the magnetic, porosity, and suction parameters.
- Nusselt number decreases for radiation, heat generation, velocity, and thermal slip parameter and increases for Prandtl number.
- Sherwood number decreases for velocity and mass slip parameter and increases for Schmidt number.
- The momentum, thermal, and concentration boundary layer thickness increase with increasing values of unsteadiness parameter.
- With increasing values of the suction parameter, the fluid velocity temperature and concentration decrease, whereas opposite behavior is seen for blowing.

References

1. N.G. Rurraswamy and B. J. Gireesha, *J. Appl. Math. Phys.* **2**, 24 (2014).
<http://dx.doi.org/10.4236/jamp.2014.22004>

2. B. C. Sakiadis, *AIChE J.* **7**, 26 (1961). <http://dx.doi.org/10.1002/aic.690070108>
3. L. J. Crane, *Zeitschrift für angewandte Mathematik und Physik ZAMP* **21**, 645 (1970).
<http://dx.doi.org/10.1007/BF01587695>
4. P. S. Gupta and A. S. Gupta, *The Canadian J. Chem. Eng.* **55**, 744 (1977).
<http://dx.doi.org/10.1002/cjce.5450550619>
5. L. J. Grubka and K. M. Bobba, *J. Heat Transf.* **107**, 248 (1985).
<http://dx.doi.org/10.1115/1.3247387>
6. E. M. Elbashbeshy, *J. Phys. D: Appl. Phys.* **31**, 1951 (1998).
<https://doi.org/10.1088/0022-3727/31/16/002>
7. H. I. Andersson, *Acta Mechanica* **158**, 121 (2002). <http://dx.doi.org/10.1007/BF01463174>
8. E. Magyari and B. Keller, *J. Phys. D: Appl. Phys.* **32**, 577 (1999).
<http://dx.doi.org/10.1088/0022-3727/32/5/012>
9. E. M. A. Elbashbeshy, *Arch. Mechanics* **53**, 643 (2001).
10. M. K. Partha, P. V. S. N. Murthy, and G. P. Rajasekhar, *Heat Mass Transf.* **41**, 360 (2005).
<http://dx.doi.org/10.1007/s00231-004-0552-2>
11. E. Sanjayanand and S. K. Khan, *Int. J. Thermal Sci.* **45**, 819 (2006).
<http://dx.doi.org/10.1016/j.ijthermalsci.2005.11.002>
12. N. Kishan, C. Kalyani, and M. C. K. Reddy, *Transp Phenom Nano Micro Scales* **4**, 44 (2016).
<http://dx.doi.org/10.7508/tpnms.2016.01.006>
13. S. K. Nandy, S. Sidui, and T. R. Mahapatra, *Alexandria Eng. J.* **53**, 929 (2014).
<http://dx.doi.org/10.1016/j.aej.2014.09.001>
14. P. C. sekar, S. Ganesh, A. M. Ismail, and C. K. Kirubhashankar, *Appl. Math. Sci.* **9**, 1509 (2015). <http://dx.doi.org/10.12988/ams.2015.5132>
15. S. Hussain and F. Ahmad, *Sci. Int. (Lahore)* **27**, 853 (2015).
16. I. C. Mandal and S. Mukhopadhyay, *Ain Shams Eng. J.* **4**, 103 (2013).
<http://dx.doi.org/10.1016/j.asej.2012.06.004>
17. S. Mukhopadhyay, *Ain Shams Eng. J.* **4**, 485 (2013). <http://doi.org/10.1016/j.asej.2012.10.007>
18. K. Bhattacharyya, S. Mukhopadhyay, and G. C. Layek, *Ain Shams Eng. J.* **4**, 299 (2013).
<http://dx.doi.org/10.1016/j.asej.2012.09.003>
19. P. Sreenivasulu, T. Poornima, and N. B. Reddy, *J. Appl. Fluid Mechanics* **9**, 267 (2016).
<https://doi.org/10.18869/acadpub.jafm.68.224.20368>
20. A. S. Zaman, A. S. A. Aziz, and Z. M. Ali, *J. Phys. Conf. Series* **890**, ID 012020 (2017).
<https://doi:10.1088/1742-6596/890/1/012020>
21. S. Chaudhary and M. K. Chaudhary, *Thermal Sci.* **22**, 797 (2018).
<https://doi.org/10.2298/TSCI160127150C>
22. M. Q. Brewster, *Thermal Radiative Transfer and Properties* (John Wiley & Sons, New York, 1992).